INT. J. REMOTE SENSING, 2003, VOL. 24, NO. 6, 1237–1258

Performance evaluation of spatial interpolation methods in the presence of noise

M. DEMIRHAN*, A. ÖZPINAR and L. ÖZDAMAR†

Yeditepe University, Department of Systems Engineering, 26 Agustos Yerleşimi, 81120 Kayisdagi, Istanbul, Turkey

(*Received 1 July 1999; in final form 19 December 2001*)

Abstract. This study aims to investigate the robustness of some spatial interpolation methods (SIM) in the presence of noisy data. SIM are used in different contexts such as the identification of hot-spots in brown fields, Geographical Information Systems (GIS), remote sensing and visualization/shape re-construction. In all contexts, the correct representation of a given surface is crucial. For instance, in a site characterization context identifying hot-spots, all contaminated areas should be determined in order to minimize health hazards in human use after the reclamation of the site. Here, we conduct a numerical survey on the performance of four spatial interpolation techniques using eight mathematical functions to represent domain-independent surfaces. Furthermore, we also investigate the effects of different sampling patterns on the performance of SIM.

1. Introduction

Interpolation techniques are utilized in many contexts including the identification of contaminated zones in potentially contaminated sites, and image re-construction or visualization, e.g. medical imaging, remotely sensed satellite imagery, identification of mining resources, topographical mapping and Geographical Information Systems (GIS) or Digital Elevation Modelling (DEM) (USGS 1987, Hutchinson 1997). Based on the specific area in which they are used, these methods are called 'geostatistical tools', 'GIS methods', or 'DEM'. The most general term for these methods is 'Spatial Interpolation Methods (SIM)' and their major assumption is that spatially closer locations are more likely to have similar observation values than those which are far apart. Foley and Hagen (1994) provide a survey on the scientific fields where SIM are used.

SIM are procedures for estimating the value of characteristics at unsampled locations within a given area in which observations exist and they are used to provide contours for displaying data graphically (DEM); to estimate some property of the surface at a given location (mining); to visualize surfaces of human organs in clinical investigation; and, to aid the spatial decision making process in detecting hot-spots (environmental assessment).

*e-mail: melekdemirhan@yahoo.com
†e-mail: lozdamar@hotmail.com

International Journal of Remote Sensing
ISSN 0143-1161 print/ISSN 1366-5901 online © 2003 Taylor & Francis Ltd
http://www.tandf.co.uk/journals
DOI: 10.1080/01431160210164325

SIM are conventional techniques used in these contexts, and they basically construct surfaces from point observations. Yet, there are uncertainties about these re-constructed surfaces due to the fact that the observed points give an indication about the surface's character at their corresponding locations, but not about the whole surface. In these methods, it is usually assumed that the value of a data point is valid for the area covered by the grid in which it lies. Among some of the problems encountered by SIM users are: (i) different interpolation algorithms yield different contours from the same data; (ii) depending on the algorithm used to contour data, the raw data are not necessarily honoured; (iii) small areas with many peak attribute levels are difficult to model using these algorithms due to their smoothing effects (Wingle 1992, Henley and Watson 1997).

A further handicap in representing surfaces is the existence of noise in the observed values. For example, in the clinical investigation of human tissues, the reliability of the data measurements obtained by ultrasound may be reduced due poor intensity contrast, speckle and shadow regions (Carr 1996); in airborne data there may be many physical factors affecting the quality of the measurements; in environmental investigations sampling errors (often, duplicate samples taken from same location result in different observation values) resulting from the sampling methodology dominate laboratory analysis errors. Consequently, a realistic performance investigation should involve data with noise. Therefore, we carry out experiments where data are distorted by additive white noise as is the case in many applications (e.g. Rauth and Ströhmer 1998). In order to demonstrate the effectiveness of the four SIM considered here, that is, multi-quadratic radial basis function, kriging, minimum curvature, and Shepherd's inverse distance method, we utilize mathematical functions to represent surfaces. We evaluate performance according to the absolute error between the true value of the given function and its corresponding interpolated value.

2. Brief descriptions of SIM considered in this study

Here we investigate the performance of four conventional SIM used in the above-mentioned contexts. (Please note that the following references indicating the use of the four SIM are just samples, and far from being exhaustive.) The first interpolator that is considered here, radial basis functions (Hardy 1990, Powel 1992), are utilized in many areas including satellite image re-construction (Fogel 1997), ultrasound imaging (Carr 1996, Rohling *et al.* 1998) and cranioplasty. The second technique, kriging, is a well-known geostatistical technique utilized in geosciences such as mining (Isaaks and Srivastava 1989, Henley and Watson 1997, Deutsch and Journel 1998), GIS (Oliver and Webster 1990, Rosenbaum and Soderstrom 1996), and in environmental site characterization (Zirschky and Harris 1986, US Army Corps of Engineers, 1997, UK DoE, 1994). The third method considered here is the minimum curvature method, which was first proposed to contour geophysical data (Briggs 1974). The minimum curvature interpolator is a commonly used geostatistical technique. The last method, Shepherd's inverse distance method, is a widely used surface fitting technique utilized in all of the above-mentioned contexts including image warping (Ruprecht and Muller 1995).

2.1. *Radial basis functions*

Radial basis functions (RBF) constitute the basis for a nonlinear transformation of a given input vector, $\mathbf{z_i} \in R^d$. Here, $\mathbf{z_i}$ are the observed locations within the surface.

Their observed values are denoted by $f(\mathbf{z_i})$. These functions are characterized by the fact that the relation between the value to be interpolated decreases monotonically with the distance from a central point (an observed data point).

The principle of a radial basis function derives from the theory of functional approximation. We consider a real valued function f, such that f: $R^d \rightarrow R$. Given the distinct set of points $\{\mathbf{z_i} \in R^d$: $i=1, 2, ..., n\}$ and their functional values $\{f(\mathbf{z_i})$: $i=1, 2, ..., n\}$, the unknown function f is to be approximated by another real valued function s: $R^d \rightarrow R$.

RBF approximations are of the form

$$s(\mathbf{z}) = \sum_{i=1}^{n} \lambda_i \phi(|\mathbf{z}-\mathbf{z_i}|) + p_m(\mathbf{z}) \quad \mathbf{z} \in R^d,\ \lambda_i \in R \tag{1}$$

where p_m is a polynomial of a low degree m, $\phi(.)$: $R^+ \rightarrow R$ is a function of the Euclidean distance between each sample data $\mathbf{z_i}$, and the given location $\mathbf{z}$ to be interpolated. Thus, the radial basis function s is a linear combination of translates of radially symmetric functions and a low degree polynomial. The coefficients λ_i are also unknown and have to be computed. If the space of all the polynomials of degree at most m in d variables is denoted by π_m^d, then the coefficients λ_i of the approximation $s(.)$ and the coefficients of the polynomial $p_m(\mathbf{z})$ are determined by requiring that $s(.)$ satisfy the following interpolation conditions,

$$s(\mathbf{z_i}) = f(\mathbf{z_i}), \quad \text{for all } i=1, 2, ..., n \tag{2}$$

and the side conditions,

$$\sum_{i=1}^{n} \lambda_i q(\mathbf{z_i}) = 0 \quad \text{for all } q \in \pi_m^d \tag{3}$$

where $q(\mathbf{z_i})$ denotes a multivariate polynomial of degree m. These side conditions enforce that the data span the space R^d, in order to constrain the polynomial $p_{\mathrm{m}}(\mathbf{z})$.

Usually a function $\phi(.)$ which has its maximum at a distance of zero is used. The popular choices of $\phi(.)$ employed are linear, Gaussian, multi-quadratic, and thin-plate splines functions (Powel 1992).

The choice of $\phi(.)$ is determined by the dimension of the problem d, the interpolation conditions and the desired properties of the interpolant. Table 1 specifies conditions for various radial basis interpolants. Here, we choose the multi-quadratic RBF because it is reported to provide excellent results in image re-construction (Fogel 1997).

2.2. *Kriging*

Kriging (originated by Krige (1951) and developed by Matheron (1971)) is a popular interpolation method used by practitioners in various fields, such as mining,

Table 1. Conditions imposed on data for various radial basis interpolants.

ϕ	Spatial dimension d	Polynomial degree m	Restriction on data
Linear	any	1	data not coplanar
Thin-plate	2	1	data not colinear
Gaussian	any	–	none
Multi-quadratic	any	–	none

Table 2. Performance of four sampling patterns using the kriging interpolation method.

	Noise-Free				Additive Gaussian Noise			
Kriging pattern	Herringbone	Grid	Linear	Circular	Herringbone	Grid	Linear	Circular
Average error	7.60	6.20	10.97	18.45	92.50	101.18	111.16	99.75
SD	10.39	8.77	23.06	46.21	73.68	71.82	79.44	76.92

geographical mapping, and environmental assessment of sites. The idea is to consider all observations as a realization of a random spatial process. The following constitute the steps taken prior to generate the interpolated grid by kriging.

Initially, the spatial variability is analysed and expressed by a function called variogram, γ, which can be estimated from the data according to the following semi-variance equation:

$$\gamma(h) = \sum_{i,\, j \in H} [f(\mathbf{z_i}) - f(\mathbf{z_j})]^2 / 2N(h) \tag{4}$$

where $N(h)$ is the number of observations separated by a distance h, and H is the set of observations h distance apart.

The above experimental variogram is used to construct a theoretical one by applying linear least squares method and thus estimating the parameters of the theoretical variogram. There are several models that can be used for the theoretical variogram: Gaussian, exponential, spherical and linear. (After preliminary experiments, here, the linear variogram is selected, because no significant differences exist in the performances of the linear variogram and the other three variogram types.) Given the theoretical variogram the question is how can the value of an unobserved location be predicted based on n observed values. Kriging deals with finding the best linear unbiased predictor.

The mathematics of kriging is described in detail by Deutsch and Journel (1998). The kriging algorithm provides a minimum error variance of any unsampled value. Contouring a grid of kriging estimates is the traditional mapping application of kriging which tends to smooth out details and extreme values of the original dataset.

Consider the unbiased estimate $f(\mathbf{z})$ from neighbouring data values $f(\mathbf{z_i})$, $i = 1 \ldots n$. The model $f(\mathbf{z})$ is stationary with mean m and covariance $C(\mathbf{h})$. The covariance is related to the semi-variogram by the following expression:

$$2\gamma(\mathbf{h}) = \mathrm{Var}[f(\mathbf{z_i} + \mathbf{h}) - f(\mathbf{z_i})] = 0.5[C(\mathbf{0}) - C(\mathbf{h})] \text{ for all } \mathbf{z_i} \tag{5}$$

where $C(\mathbf{0})$ is the stationary variance. In its simplest form, also known as simple kriging, the algorithm considers the following linear estimator.

$$\overset{n}{\underset{i=1}{f'}}(\mathbf{z}) = \sum \lambda_i(\mathbf{z}) f(\mathbf{z_i}) + [1 - \sum \lambda_i(\mathbf{z})]m \tag{6}$$

where f' is the linear regression estimator and m is the known mean value. The simple kriging weights $\lambda_i(\mathbf{z})$ are determined to minimize the error variance also called 'estimation variance'(Luenberger 1969).

The minimized estimation variance or kriging variance is

$$\sigma^2(\mathbf{z}) = C(0) - \sum_{i=1}^{n} \lambda_i(\mathbf{z}) C(\mathbf{z} - \mathbf{z_i}) \geqslant 0 \tag{7}$$

The latter minimization results in the following normal equations from which the optimal weights $\lambda_j(\mathbf{z})$ are calculated.

$$\sum_{j=1}^{n} \lambda_j(\mathbf{z}) C(\mathbf{z_j} - \mathbf{z_i}) = C(\mathbf{z} - \mathbf{z_i}), \quad \text{for all } i = 1 \ldots n \tag{8}$$

There are several versions of kriging resulting in different topologies. All of them are elaborations on a basic generalized regression algorithm and the corresponding estimator. Here, ordinary kriging (OK) which relaxes the constraint of the stationary mean, is selected for the experimentation. OK, where the sum of the weights is equal to 1, is the most commonly used variant of the simple kriging algorithm described above. OK allows building an estimator that does not require prior knowledge of the stationary mean m which is replaced by its location-dependent estimate. Hence, the mean value m is filtered out since $\Sigma_j \lambda_j(\mathbf{z}) = 1$. OK amounts to re-estimating the mean m as used in the simple kriging expression at each new location $\mathbf{z} = (x, y)$. Thus, it is a non-stationary algorithm in the sense that it corresponds to a non-stationary model with varying mean and stationary covariance.

2.3. *Minimum curvature*

The minimum curvature method has first been proposed by Briggs (1974) for automatic contouring of geophysical data. Here, a two-dimensional cubic spline is employed to fit the data by solving the corresponding difference equations with the objective of keeping the total squared curvature minimum. The interpolated surface generated by minimum curvature is analogous to a thin linearly elastic plate passing through each of the data values with a minimum amount of bending. Minimum curvature generates the smoothest possible surface while attempting to honour the data as close as possible, but it is not an exact interpolator and replaces the observation value by the interpolated value should they fall upon the same location.

For $d = 2$, the curvature is obtained in terms of the observation point values $f(x_i, y_j)$, $i = 1 \ldots I$; $j = 1 \ldots J$, where I and J are the numbers of grids in the x- and y-directions. The curvature depends on the regular grid spacing of observations h. The total squared curvature $C = \Sigma_i \Sigma_j C(x_i, y_j)^2$, where

$$C(x_i, y_j) = [f(x_i, y_{j+1}) + f(x_i, y_{j-1}) + f(x_{i-1}, y_j) + f(x_{i+1}, y_j) - 4f(x_i, y_j)]/h^2 \tag{9}$$

Here, $f(.)$ denotes the observed value if its arguments, x and y, coincide with locations of observed data, else, it represents a cubic polynomial within which the coordinates of the point to be interpolated are substituted.

The local coefficients of the cubic polynomial are calculated by minimizing the total squared curvature C where the partial derivatives of C with respect to $f(x_i, y_j)$ are set to zero. The resulting equations determine a set of relations between neighbouring locations and they are solved to identify the coefficients of the cubic polynomial. If one of the vertices does not coincide with an observation, then additional difference equations are used for the missing vertex. The resulting system of equations are then solved iteratively.

2.4. *Shepherd's inverse distance method*

In the inverse distance method, the value of a point to be interpolated is calculated by taking the weighted average of neighbouring observations. The weight of each observation is a function of the inverse of the Euclidean distance between the

observation and the interpolated location. In general terms, the interpolated value is expressed as follows.

$$\sum_i [f(\mathbf{z_i}) d_i^{-p}] / \sum_i d_i^{-p} \tag{10}$$

where p is a power selected by the user, and d_i is the Euclidean distance between observation i and the location of the interpolated point. The higher the value of p is, the larger the effect of the closer points become. Here, we employ the conventional value of two for the parameter p. If the sum of the weights is equal to one and if an interpolated value takes the value of an observation in case of coincident coordinates, then inverse distance method can be classified as an exact interpolator.

3. The test functions

Eight test functions are devised to illustrate various possible characteristics of hypothetical surface patterns on which the performance of SIM are to be evaluated. Initially, SIM are utilized to approximate the behaviours of the original forms of the functions based on a given number of sample data. (Here, 196 samples are collected.) Then, the surface of each function is distorted with additive Gaussian noise (noise is generated in proportion to the range of function values pertaining to 196 data) and the performances of SIM are re-evaluated.

The three-dimensional images of the test functions are provided in Appendix A (figures A1–A8). The first test function represents a plateau type of surface where sharp falls occur near the corners. The second, third, fourth and the fifth test functions (see figures A2–A5) are generated according to the scheme described in Stuckman (1988). The forth function represents very sharp stepwise changes of attribute level whereas the fifth one involves stepwise changes of smaller magnitudes, thus presenting a smoother surface. The second one (figure A2) is again a discontinuous function where changes are relatively smoother except at one corner of the site. Furthermore, when the steps of the second function are removed, a very slightly undulating function (figure A3) results. The sixth test function is a symmetric function with very frequent changes in attribute levels achieved over small distances. The seventh function has a trend in attribute level and a relatively lower number of extremities. On the opposite hand, the eight one has many extremities in between which there lie plateaus and valleys.

4. The sampling patterns

We implement the following four different sampling patterns: herringbone, regular grid, linear type and circular sampling (see figure 1).

The herringbone sampling pattern (Ferguson 1992) can be generated from a unit

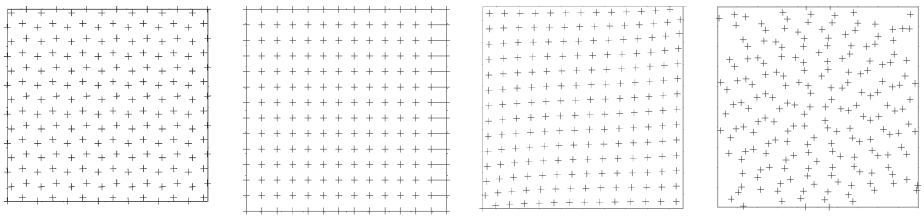

Figure 1. Four sampling patterns.

square grid by offsetting data points one quarter of a unit from the centre of the grid, in the x- and y-coordinates in a systematically alternating manner. Thus, each area unit includes one observation. The number of area units is hence equal to the number of observations to be made on the given surface. It is claimed to be quite efficient in the contaminated zone detection context (UK DoE, 1994).

The regular grid sampling pattern is generated by dividing the surface into a number of rectangular units and placing one observation at the centre of each such unit. The regular grid provides a uniform cover over the surface.

The linear sampling pattern is generated by placing observations on k parallel equidistant lines drawn across the surface. These lines divide the surface into equidistant cross-sections and each makes an angle of 45° with the x-axis. The first line contains a single observation while the second one contains two observations. In this manner, the number of observations on each line becomes equivalent to its index until $k/2$ lines are drawn. Then, the number of observations in each succeeding line decreases by one. Hence, given a fixed number of observations, n, the number of equidistant lines to be drawn in parallel can be calculated easily.

In the circular sampling pattern, the first observation is placed at the geometric centre of the surface. Similar to the linear pattern, one more observation is added to each additional circle drawn around the centre of the surface. However, in order to eliminate aligned positions, the first observation on each circle is offset by a given degree from the last observation placed on the previous circle. The degree of offsetting is computed by dividing 360° by the number of circles to be drawn.

5. Distorting function values by additive white noise

The noise that is added to original function values of observations is generated as follows. A number of observation locations are generated across the site area according to a given sampling pattern and their corresponding function values are calculated. Then, the range, R, of function values over the whole sample set is determined. A normal additive noise is randomly generated with mean zero and standard deviation equal to $0.1R$.

That is, for any location $\mathbf{z_i}$, the distorted observation $f(\mathbf{z_i})$ is given by,

$$f'(\mathbf{z_i}) = f(\mathbf{z_i}) + \varepsilon_i \quad \text{for } i = 1, 2, \ldots n \tag{11}$$

where $\varepsilon_i \sim N(0, 0.1R)$ and n is the number of location points generated.

The interpolation error, IE_i, is taken as the absolute difference between the interpolated value, and $f(\mathbf{z_i})$.

6. An example demonstrating the distortion caused by additive white noise

The test function depicted in figure A1 is used to demonstrate the distortion of the surface's shape caused by white noise. In figure 2 the contours of the function are shown. In figure 3(*a*)–(*d*), the surfaces interpolated by kriging using the four sampling methods are given. The last set of four contours (figure 3(*e*)–(*h*)) are the corresponding interpolated surfaces when noise is added to the data. Table 2 provides the average and standard deviation of the interpolation errors, IE_i obtained by the four sampling patterns using the Kriging interpolation method (50×50 grid). Although the regular grid pattern provides the minimum average absolute value, its performance in the presence of noise is intolerable (see figure 3(*b*) and (*f*)). When the data are noise-free, 81% of the interpolation errors are within 1% of the function's

Table 3. Interpolation error results for function 1.

	Without Gaussian noise					With Gaussian noise				
	Herringbone	Grid	Linear	Circular	Method avg	Herringbone	Grid	Linear	Circular	Method avg
Kriging										
Avg	7.604	6.207	10.974	18.452	10.809	92.500	101.182	111.156	99.747	101.146
SD	10.389	8.768	23.060	46.215	22.108	73.681	71.826	79.443	76.916	75.467
Minimum curvature										
Avg	12.531	10.349	10.749	23.228	14.214	112.269	118.024	130.308	137.974	124.644
SD	12.879	10.411	15.516	52.605	22.853	87.204	81.299	99.885	100.721	92.277
Radial basis										
Avg	5.115	4.653	8.340	14.281	8.097	115.803	116.245	122.636	116.366	117.762
SD	9.007	7.762	19.756	39.194	18.930	85.587	82.221	90.150	84.241	85.550
Shepard's										
Avg	106.365	105.189	99.005	140.480	112.760	124.143	120.540	118.540	152.478	128.925
SD	63.320	61.871	68.546	122.868	79.151	77.758	79.782	89.217	168.602	103.840
Sample avg	32.904	31.600	32.267	49.110	36.470	111.179	113.998	120.660	126.641	118.119
Sample SD	23.899	22.203	31.719	65.220	35.760	81.058	78.782	89.674	107.620	89.283
Range	1811.65	1604.70	1494.80	2144.94	1764.022	1909.87	1528.52	1591.52	2203.83	1808.435

Table 4. Interpolation error results for function 2.

	Without Gaussian noise					With Gaussian noise				
	Herringbone	Grid	Linear	Circular	Method avg	Herringbone	Grid	Linear	Circular	Method avg
Kriging										
Avg	1.647	1.714	1.672	1.742	1.694	2.152	2.244	2.251	2.417	2.266
SD	2.233	2.591	2.756	3.209	2.697	2.382	2.501	2.652	3.636	2.793
Minimum curvature										
Avg	1.763	1.722	1.692	2.300	1.869	2.643	2.470	2.617	2.817	2.637
SD	2.346	2.623	2.659	3.953	2.895	2.463	2.396	2.992	4.214	3.016
Radial basis										
Avg	1.658	1.732	1.600	1.888	1.720	2.399	2.456	2.381	2.755	2.498
SD	2.335	2.672	2.721	3.185	2.728	2.400	2.420	2.696	3.863	2.845
Shepard's										
Avg	2.924	2.956	2.825	3.178	2.971	3.278	3.278	2.942	3.330	3.207
SD	2.707	2.974	2.486	3.214	2.845	2.618	2.982	2.512	3.432	2.886
Sample Avg	1.998	2.031	1.948	2.277	2.063	2.618	2.612	2.548	2.830	2.652
Sample SD	2.405	2.715	2.656	3.390	2.792	2.466	2.575	2.713	3.786	2.885
Range	49.45	48.69	47.52	49.84	48.873	47.81	47.72	47.91	49.06017	48.125

Table 5. Interpolation error results for function 3.

	Without Gaussian noise					With Gaussian noise				
	Herringbone	Grid	Linear	Circular	Method avg	Herringbone	Grid	Linear	Circular	Method avg
Kriging										
Avg	0.073	0.059	0.106	0.329	0.142	1.735	1.731	1.886	2.155	1.877
SD	0.106	0.077	0.228	0.816	0.307	1.409	1.437	1.525	2.153	1.631
Minimum curvature										
Avg	0.287	0.291	0.283	0.362	0.306	2.195	2.292	2.188	2.598	2.318
SD	0.319	0.319	0.352	0.593	0.396	1.809	1.743	1.931	2.434	1.979
Radial basis										
Avg	0.042	0.039	0.082	0.236	0.100	2.201	2.069	2.153	2.582	2.251
SD	0.083	0.082	0.187	0.669	0.255	1.587	1.692	1.688	2.103	1.767
Shepard's										
Avg	2.483	2.547	2.407	3.421	2.714	3.175	3.109	2.951	4.098	3.333
SD	1.933	1.932	1.792	3.608	2.316	2.223	2.133	2.050	5.040	2.861
Sample avg	0.721	0.734	0.719	1.087	0.815	2.326	2.300	2.294	2.858	2.445
Sample SD	0.610	0.603	0.640	1.422	0.818	1.757	1.751	1.798	2.932	2.060
Range	73.11	66.22	69.87	72.77	70.491	72.24	67.22	68.20	77.75827	71.355

Table 6. Interpolation error results for function 4.

	Without Gaussian noise					With Gaussian noise				
	Herringbone	Grid	Linear	Circular	Method avg	Herringbone	Grid	Linear	Circular	Method avg
Kriging										
Avg	0.126	0.125	0.154	0.151	0.139	0.168	0.171	0.214	0.197	0.187
SD	0.138	0.155	0.225	0.192	0.178	0.134	0.154	0.235	0.213	0.184
Minimum curvature										
Avg	0.126	0.133	0.191	0.161	0.153	0.176	0.185	0.235	0.223	0.205
SD	0.139	0.148	0.251	0.209	0.187	0.140	0.158	0.254	0.230	0.196
Radial basis										
Avg	0.126	0.125	0.170	0.155	0.144	0.167	0.179	0.220	0.219	0.196
SD	0.133	0.142	0.205	0.192	0.168	0.144	0.160	0.232	0.238	0.194
Shepard's										
Avg	0.215	0.205	0.225	0.239	0.221	0.234	0.227	0.253	0.264	0.245
SD	0.159	0.165	0.228	0.207	0.190	0.158	0.159	0.212	0.191	0.180
Sample Avg	0.148	0.147	0.185	0.177	0.164	0.186	0.190	0.231	0.226	0.208
Sample SD	0.142	0.152	0.227	0.200	0.180	0.144	0.158	0.233	0.218	0.188
Range	2.04	2.13	2.01	2.05	2.058	2.14	2.00	2.03	2.1085915	2.069

Table 7. Interpolation error results for function 5.

	Without Gaussian noise					With Gaussian noise				
	Herringbone	Grid	Linear	Circular	Method avg	Herringbone	Grid	Linear	Circular	Method avg
Kriging										
Avg	0.649	0.610	0.612	0.760	0.658	0.950	0.958	1.009	1.149	1.017
SD	0.779	0.835	0.798	1.066	0.869	0.857	0.913	0.816	1.150	0.934
Minimum curvature										
Avg	0.671	0.695	0.727	1.016	0.777	1.161	1.157	1.175	1.511	1.251
SD	0.858	0.895	0.852	1.561	1.042	0.941	0.998	1.045	1.511	1.124
Radial basis										
Avg	0.641	0.678	0.596	0.840	0.689	1.024	1.089	1.088	1.301	1.126
SD	0.808	0.763	0.763	1.048	0.846	0.909	0.918	0.927	1.216	0.993
Shepard's										
Avg	1.121	1.015	1.067	1.436	1.160	1.273	1.202	1.161	1.532	1.292
SD	0.963	0.803	0.800	1.135	0.925	0.975	0.889	0.875	1.178	0.979
Sample avg	0.770	0.749	0.751	1.013	0.821	1.102	1.101	1.108	1.373	1.171
Sample SD	0.852	0.824	0.803	1.203	0.920	0.920	0.929	0.916	1.264	1.007
Range	13.37	9.72	9.92	14.45	11.864	13.62	10.48	9.92	14.3122	12.085

Table 8. Interpolation error results for function 6.

	Without Gaussian noise					With Gaussian noise				
	Herringbone	Grid	Linear	Circular	Method avg	Herringbone	Grid	Linear	Circular	Method avg
Kriging										
Avg	5.008	4.492	4.829	5.029	4.840	10.722	9.844	10.441	11.045	10.513
SD	4.191	4.144	4.028	4.566	4.232	8.016	8.322	7.791	8.720	8.212
Minimum curvature										
Avg	4.868	4.763	5.317	6.612	5.390	11.846	11.291	12.690	15.662	12.872
SD	4.402	4.391	5.480	6.344	5.154	9.352	8.730	10.990	15.111	11.046
Radial basis										
Avg	4.926	4.928	4.856	5.608	5.080	12.322	11.989	11.613	13.225	12.287
SD	4.309	4.289	4.394	4.929	4.480	9.645	8.959	8.947	10.289	9.460
Shepard's										
Avg	4.819	4.786	4.669	5.005	4.820	8.373	8.374	8.072	8.811	8.407
SD	3.698	3.885	3.455	3.928	3.742	7.092	7.335	6.620	9.376	7.605
Sample avg	4.905	4.743	4.918	5.563	5.032	10.816	10.374	10.704	12.186	11.020
Sample SD	4.150	4.177	4.339	4.942	4.402	8.526	8.336	8.587	10.874	9.081
Range	26.92	26.83	25.42	27.83	26.748	27.02	27.91	27.19	28.28235	27.600

Table 9. Interpolation error results for function 7.

	Without Gaussian noise					With Gaussian noise				
	Herringbone	Grid	Linear	Circular	Method avg	Herringbone	Grid	Linear	Circular	Method avg
Kriging										
Avg	1.742	1.655	1.661	2.816	1.969	3.542	3.152	3.386	4.724	3.701
SD	2.001	1.781	2.029	4.347	2.539	2.747	2.422	2.784	5.256	3.302
Minimum curvature										
Avg	1.406	1.272	1.389	2.644	1.678	3.775	3.492	3.895	5.246	4.102
SD	1.735	1.594	2.782	5.000	2.778	2.883	2.891	4.240	7.267	4.320
Radial basis										
Avg	1.074	1.028	1.024	2.411	1.384	3.663	3.341	3.602	4.666	3.818
SD	1.364	1.343	1.678	4.057	2.110	2.544	2.652	2.925	4.739	3.215
Shepard's										
Avg	4.075	3.956	4.138	6.692	4.715	4.837	4.423	4.538	8.513	5.578
SD	4.524	4.340	4.696	10.581	6.035	4.546	4.101	4.593	13.617	6.714
Sample avg	2.074	1.977	2.053	3.641	2.436	3.954	3.602	3.855	5.787	4.300
Sample SD	2.406	2.264	2.796	5.996	3.366	3.180	3.017	3.635	7.720	4.388
Range	219.99	200.79	219.99	200.79	210.391	225.64	199.74	225.64	199.74	212.693

Table 10. Interpolation error results for function 8.

	Without Gaussian noise					With Gaussian noise				
	Herringbone	Grid	Linear	Circular	Method avg	Herringbone	Grid	Linear	Circular	Method avg
Kriging										
Avg	0.191	0.195	0.172	0.290	0.212	0.315	0.291	0.337	0.405	0.337
SD	0.198	0.206	0.188	0.351	0.236	0.232	0.234	0.252	0.354	0.268
Minimum curvature										
Avg	0.192	0.179	0.182	0.299	0.213	0.338	0.341	0.380	0.518	0.394
SD	0.216	0.204	0.224	0.477	0.280	0.305	0.265	0.290	0.631	0.373
Radial basis										
Avg	0.174	0.170	0.159	0.271	0.194	0.342	0.313	0.366	0.431	0.363
SD	0.188	0.191	0.189	0.355	0.231	0.249	0.273	0.260	0.365	0.287
Shepard's										
Avg	0.300	0.275	0.304	0.368	0.312	0.355	0.359	0.376	0.437	0.382
SD	0.293	0.315	0.319	0.439	0.342	0.319	0.314	0.346	0.420	0.350
Sample avg	0.214	0.205	0.204	0.307	0.233	0.337	0.326	0.365	0.448	0.369
Sample SD	0.224	0.229	0.230	0.405	0.272	0.276	0.271	0.287	0.442	0.319
Range	5.37	5.15	4.89	5.82	5.308	5.54	5.22	5.04	6.000356	5.449

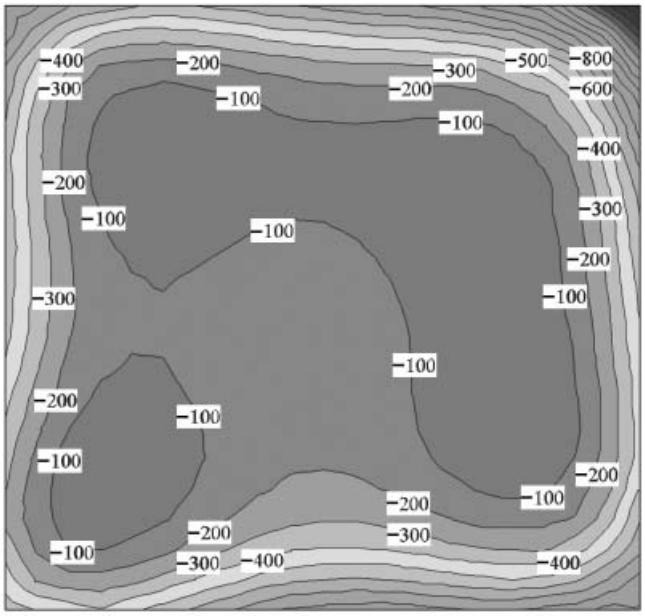

Figure 2. The original contours of the function.

range over the defined domain. On the other hand, when noise is added, only 20% of the errors fall within this range.

7. Numerical experiments with SIM

The test functions provide our medium of experimentation. Observations are made on the surface domains given for each function according to each of the four sampling patterns described in figure 1. Interpolation is then applied to each function in both cases where the original and the distorted observation values (196 data for each function domain) are utilized as functional information. In tables 3–10 each function's interpolation error results are provided under four interpolation methods and four sampling patterns. The performance of each SIM is measured in terms of both absolute error and percentage error. However, percentage error details are not given here due to space restrictions. The first two rows in each table indicate average and standard deviation of the absolute difference of interpolated values from the original function values. (The number of interpolated points is equal to 2500 resulting from a 50×50 grid.) The numbers indicated under the column 'method average' provide the average results obtained by each method over the four sampling patterns. The rows starting with 'sample average' indicate the average results of each sampling pattern over four SIM. The third row under the 'sample average' provides the range of the function values (over the 2500 interpolated locations) so that the reader can compare average absolute errors against this range. The implementation of kriging is carried out as follows. A linear variogram is used for all functions and sampling patterns. Anisotropic effects are ignored since introducing directional effects on the variogram may confound the effects of different sampling patterns on interpolation results. Further, our experiments are conducted with no assumptions related to the

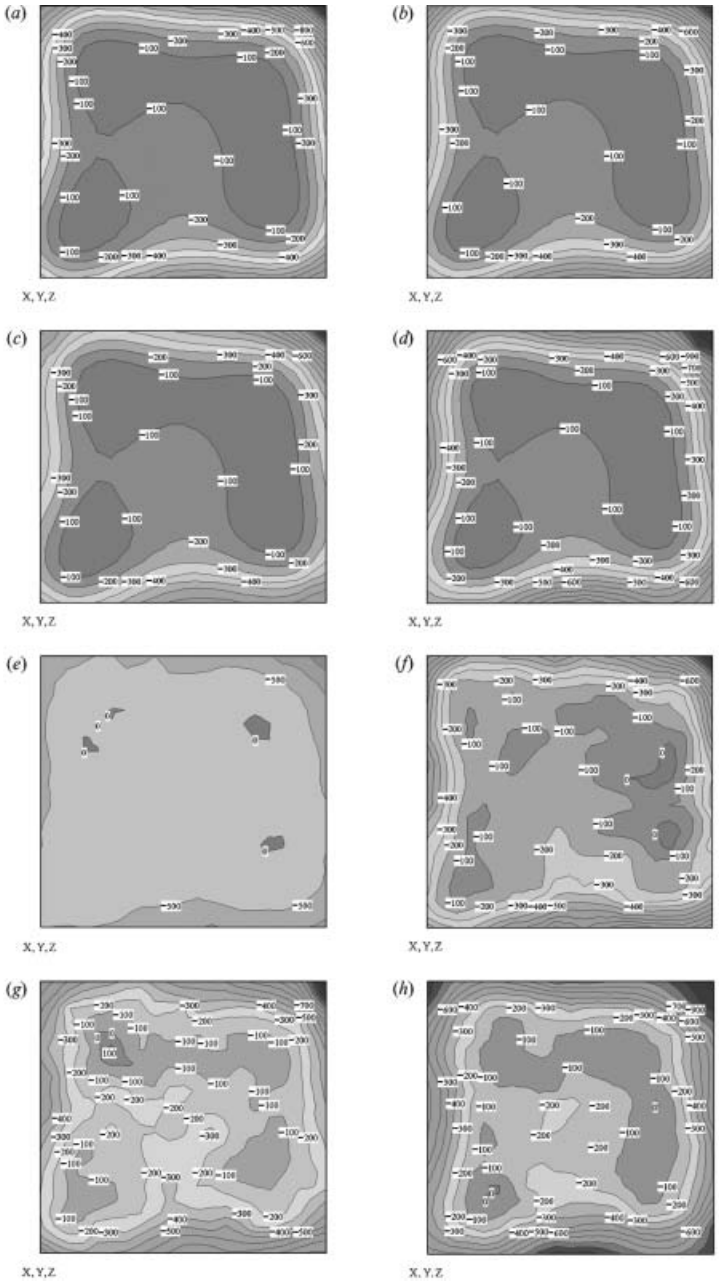

Figure 3. Kriging. (*a*) Herringbone sampling pattern/noise-free, (*b*) grid sampling pattern/noise-free, (*c*) linear sampling pattern/noise-free, (*d*) circular sampling pattern/noise-free, (*e*) herringbone sampling pattern/with noise, (*f*) grid sampling pattern/with noise, (*g*) linear sampling pattern/with noise, (*h*) circular sampling pattern/with noise.

functions used to simulate the site. Another parameter in kriging is the search window. Since the number of data used is not large, all data are utilized in interpolating a location. The nugget effect is neglected in both noise-free and noise cases, because it is assumed that no pre-determined information is available.

When there is no Gaussian noise in the data, Shepherd's method provides worst performances except the third and sixth function.

The performance of minimum curvature is considerably superior to that of Shepherd's. However, it is the third SIM in terms of performance. The performance of RBF is alternatingly the best or second best. At times kriging is slightly superior to RBF. However, when RBF is superior to kriging, differences between the two methods are considerable. RBF performs specifically well for smooth functions where abrupt changes do not take place (e.g. functions 1, 3, 7). On the other hand, when noise is included in the data kriging's performance is superior to that of RBF. Thus, kriging turns out to be more robust method against noise.

Considering the differences of sampling patterns (again excluding noise from data), the circular sampling pattern is the worst because it does not cover the site uniformly. The grid and linear patterns behave in a similar manner. The herringbone pattern follows closely the latter two patterns. Consequently, in the noise-free case, patterns covering uniformly cover the domain work better.

In the case where noise is included, the regular grid is again the best performing sampling pattern and the linear pattern is a close second. The herringbone and circular patterns share the worst performing position. Consequently, the regular grid seems to be the most robust sampling pattern against white noise.

8. Conclusion

In this work we conduct experiments to assess the performance of spatial interpolation methods in the presence of noisy data and for sampling patterns: two well-known sampling patterns as well as two novel ones introduced here.

The experiments are conducted on a test bed of eight mathematical functions and it is observed that the simplest sampling pattern, namely, the regular grid, is the most robust sampling pattern. Furthermore, among the four spatial interpolation techniques tested here, kriging is the most robust one against noise whereas the multi-quadratic RBF turns out to be the best technique when observations are noise-free.

Appendix: test functions

1.

$$f(x,y) = (x^2 + y - 11)\cdot(x^2 + y - 11) - (x + y^2 - 7)\cdot(x + y^2 - 7)$$

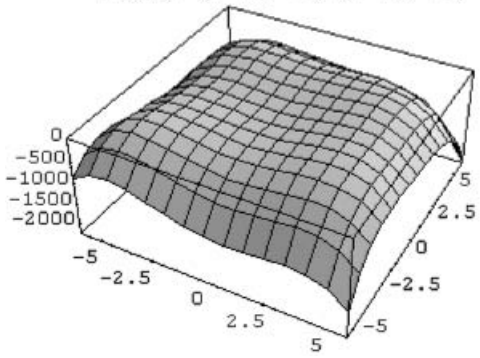

Figure A1. Function 1.

2.

$$a_1 = \text{int}(x - 1.87) + \text{int}(y - 9.3)$$

$$f(x,y) = \text{int}(75.95 + 0.5)\cdot\frac{\sin a_1}{a_1}$$

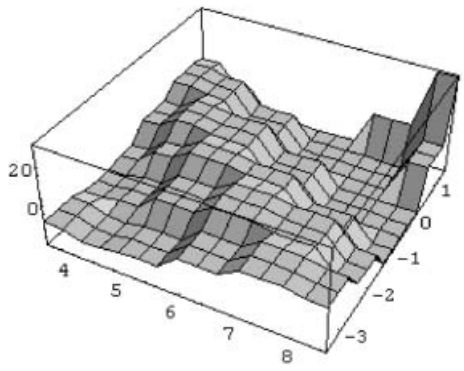

Figure A2. Function 2.

3.

$$a_1 = (x - 1.87) + (y - 9.3)$$

$$f(x,y) = (75.95 + 0.5)\cdot\frac{\sin a_1}{a_1}$$

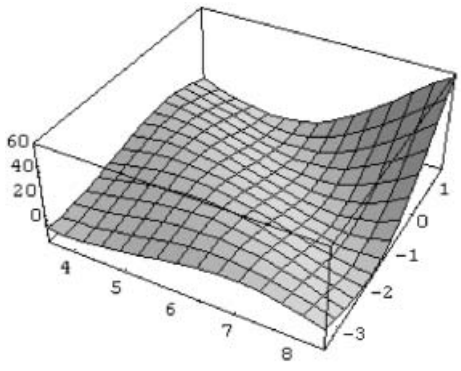

Figure A3. Function 3.

4.

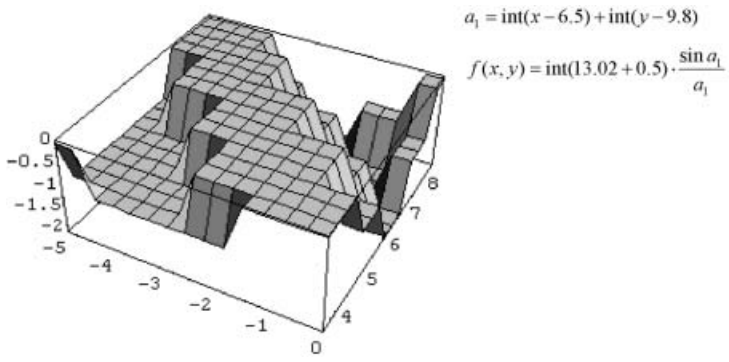

Figure A4. Function 4.

5.

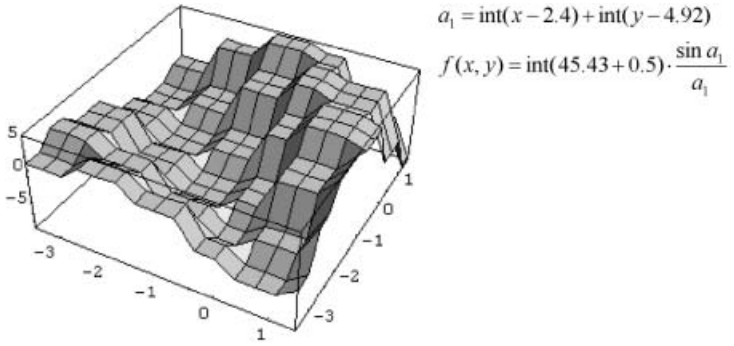

Figure A5. Function 5.

6.

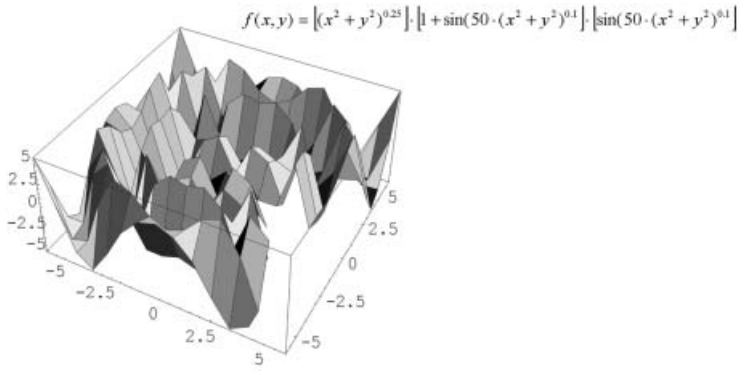

Figure A6. Function 6.

7.

$$f(x,y)=\frac{(x+2y-7)^2}{x+1}+\sin(3\cdot(2x+y-5)\cdot(x^2-y)$$

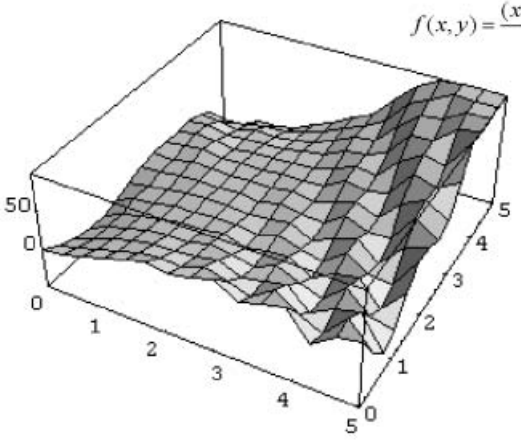

Figure A7. Function 7.

8.

$$f(x,y)=\sin(0.1\cdot(x+y)^2+1.5)\cdot\text{int}(0.5x\cdot\cos(y))$$

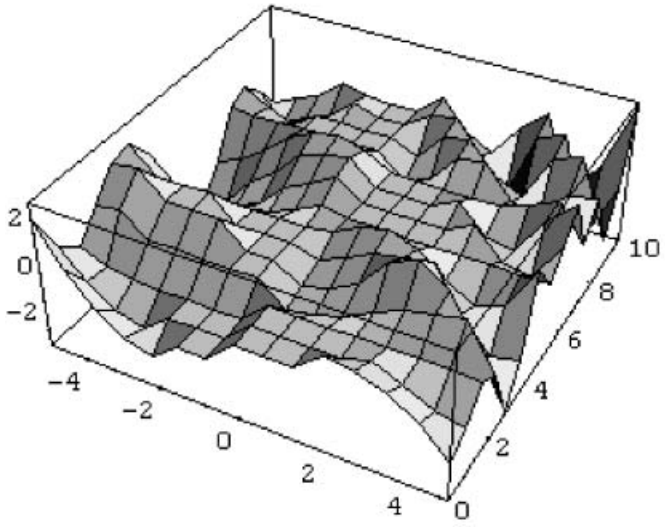

Figure A8. Function 8.

References

BRIGGS, I. C., 1974, Machine contouring using minimum curvature. *Geophysics*, **39**, 39–48.

CARR, J., 1996, Surface reconstruction in 3D medical imaging. PhD thesis, Electrical and Electronic Engineering, University of Canterbury, New Zealand.

DEUTSCH, C. V., and JOURNEL, A. G., 1998, *GSLIB: Geostatistical Software Library and User's Guide* (New York: Oxford University Press).

FERGUSON, C. C., 1992, The statistical basis for spatial sampling of contaminated land. *Ground Engineering*, **25**, 34–38.

FOGEL D. N., 1997, Image rectification with radial basis functions: application to RS/GIS data integration. Available at *htpp//polux.geog.ucsb.edu/∼ifogel/sf/santafe.html*.

FOLEY, T. A., and HAGEN, H., 1994, Advances in scattered data interpolation. *Survey on Mathematics for Industry*, **4**, 71–**84**.

HARDY, R. L., 1990, Theory and applications of multi-quadric biharmonic method. *Computers and Mathematical Applications*, **19**, 163–208.

HENLEY, S., and WATSON, D. F., 1997, Geostatistics: a critical review. Working Paper, CSIRO Exploration and Mining, Nedlands, Western Australia.

HUTCHINSON, M. F., 1997, A locally adaptive approach to the interpolation of digital elevation models. Working Paper, Australian National University, Centre for Resource and Environmental Studies, Canberra, Australia.

ISAAKS, E. H., and SRIVASTAVA, R. M., 1989, *An Introduction to Applied Geostatistics* (New York: Oxford University Press).

KRIGE, D. G., 1951, A statistical approach to some mine valuations and allied problems at Witwatersrand. MSc thesis, University of Witwatersrand, South Africa.

LUENBERGER, D., 1969, *Optimization by Vector Space Methods* (New York: John Wiley and Sons).

MATHERON, G., 1971, The theory of regionalized variables and its applications. *Les Cahier du Centre de Morphologie Mathematique*, **5**, 211–222.

OLIVER, M. A., and WEBSTER, R., 1990, Kriging: a method of interpolation for geographical information systems. *International Journal of Geographic Information Systems*, **4**, 313–332.

POWEL, M. J. D., 1992, The theory of radial basis function approximation in 1990. *Advances in Numerical Analysis*, edited by W. Light (Oxford: Oxford Science Publications), pp. 105–210.

RAUTH, M., and STRÖHMER, T., 1998, Smooth approximation of potential fields from noisy scattered data. *Geophysics*, **63**, 85–94.

ROSENBAUM, M., and SODERSTROM, M., 1996, Geostatistics as an aid to mapping. http://www.esri.com/base/common/userconf/europroc96/papers/pn11/pn11f.html.

ROHLING, R. N., GEE, A. H., and BERMAN, L., 1998. Radial basis function interpolation for 3-D ultrasound. Working Paper, Cambridge University Engineering Department, UK.

RUPRECHT, D., and MULLER, H., 1995, Image warping with scattered data interpolation. *IEEE Transactions on Computer Graphics and Applications*, **15**, 37–43.

STUCKMAN, B. E., 1988, A search method for optimizing nonlinear systems. *IEEE Transactions on Systems, Man and Cybernetics*, **18**, 965–977.

UK DoE, 1994, Contaminated land research report no. 4, Sampling strategies for contaminated land (London: Department of Environment).

US ARMY CORPS OF ENGINEERS, HTRW REPORT, 1997, Practical aspects of applying geostatistics at hazardous, toxic, and radioactive waste sites. CEMP-RT, Technical Report ETL 1110-1-175.

USGS, 1987, Digital elevation models, data users guide 5. US Department of the Interior, USGS, Reston, VA.

WINGLE, W. L., 1992, Examining common problems associated with various contouring methods particularly inverse-distance methods using shaded relief surfaces. *Geotech '92*, Lakewood, Colorado, 1992.

ZIRSCHKY, J. H., and HARRIS, D. J., 1986, Geostatistical analysis of hazardous waste site data. *Journal of Environmental Engineering*, **112**, 770–784.